The Pennsylvania State University
The Graduate School

TROPICAL CYCLONE CHANGES IN PSEUDO GLOBAL WARMING SCENARIOS

A Thesis in
Meteorology and Atmospheric Science
by
Tyrone Zhang

Submitted in Partial Fulfillment
of the Requirements
for the Degree of

Master of Science

December 2023

The thesis of Tyrone Zhang was reviewed and approved by the following:

Colin M. Zarzycki
Assistant Professor of Meteorology and Climate Dynamics
Thesis Advisor

Anthony Didlake
Associate Professor of Meteorology

Laifang Li
Assistant Professor of Meteorology and Atmospheric Science

Paul Markowski
Professor of Meteorology
Head of the Department of Meteorology and Atmospheric Science

Abstract

Tropical cyclones (TCs) are impactful weather events that disrupt economies, endanger people, and damage property. There is an urgent need to understand how these storms will change from global warming. The Weather Research and Forecasting (WRF) model was used to run one historical and two pseudo-global warming (PGW) scenarios, which were then separated into four warm scenarios, to get a better understanding of how warming impacts TCs. Using TempestExtremes to track tropical systems was successful and the data was processed to give 5 directly comparable files. Maximum precipitation and other moisture variables had an increase in all warm scenarios and many snapshots. Dynamical variables such as surface wind had a smaller increase in the warm scenarios. Different intensity TCs behave differently when looking at the changes in maximum precipitation by intensity. Furthermore, max precipitable water appears to increase in almost all snapshots when compared to the historical case. Most other variables have snapshots that decrease in value in a warmer scenario. These results support the current TC community's thoughts on the changes in TCs in a warmer world.

Table of Contents

List of Figures

List of Tables

Acknowledgments

I acknowledge Prof. Colin Zarzycki for giving me feedback, advising me through this research, and being flexible. I appreciate the folks at Lawrence Berkeley National Laboratory – particularly Dr. Andy Jones and Dr. Paul Ullrich – who ran the WRF model for these scenarios and gave us access to the data that allowed me to do this analysis. I also acknowledge Prof. William Brune and Sam Murphy for providing me with feedback on an early draft of a manuscript. Also thank you to the MEWAC research group for giving me feedback on my research. Thank you to Prof. Anthony Didlake and Prof. Laifang Li for serving on my committee and giving me feedback. Thank you to friends and family who support what I do and encourage me to do what I feel is best for me.

This work was supported by the U.S. Department of Energy, Office of Science, Office of Biological and Environmental Research program under Award DE-SC0016605 "A framework for improving analysis and modeling of Earth system and intersectoral dynamics at regional scales." The findings and conclusions of this study do not necessarily reflect the views of the DOE

Chapter 1
Introduction

1.1 Introduction

Tropical cyclones (TCs) are one of the most destructive weather events on Earth. When TCs make landfall, they bring heavy rain, wind, and storm surge. This results in property being damaged, economic activity being interrupted, and livelihoods being harmed (Mendelsohn et al., 2012). TC impacts will only increase as the population rises along coastal areas, which are vulnerable to TCs (Smith & Katz, 2013). Thus, it is crucial to understand the impacts of climate change on the characteristics of TCs, as understanding what aspects of TCs are changing can help us better prepare for future TCs in a warmer climate.

Many factors can impact the intensity of TCs. The first factor is sea surface temperatures (SST). Typically as long as the SST is above 26°C, the ocean provides sufficient energy to the TC to maintain or intensify its strength (Gray, 1968). There are some exceptions to this, such as hybrid systems that transition into TCs over SSTs lower than 26°C based on baroclinicity (C. A. Davis & Bosart, 2003). It is also worth noting that SSTs provide an upper bound to the intensity of TCs and do not predict whether a TC intensifies or not (DeMaria & Kaplan, 1994). Another factor that affects TC strength is wind shear. Wind shear is the difference in wind vectors between two vertical levels of the atmosphere (commonly 250 hPa and 850 hPa for TCs). Wind shear can help disrupt the TC structure and vortex, which exposes the TC to potentially an unfavorable environment, like dry air. Wind shear can be a key hurdle that could prevent TCs from strengthening and can help weaken TCs. Also, wind shear helps decrease the certainty of forecasts of TC intensity (K. Emanuel et al., 2004), which can make it difficult to communicate forecasts to the public. Other factors, including a favorable thermodynamic environment for deep convection, moist mid-level troposphere, and upper-level divergence,

can help TCs intensify, although none of these factors are sufficient for the TC to intensify (Gray, 1968). Furthermore, there are internal processes such as eyewall replacement cycles that can help temporarily weaken TCs, as well as going over land which always weakens TCs.

1.2 Previous studies on TC changes from climate change

With high SSTs being the key source of energy that sustains TCs, higher SSTs may help make TCs more intense in a warmer world (DeMaria & Kaplan, 1994). This would be consistent with the potential intensity theory, which is a theoretical model of the maximum intensity a TC could obtain given SSTs and the tropopause potential temperature to yield a minimum pressure (K. A. Emanuel, 1986). Using the potential intensity theory, higher SSTs do correlate with more intense TCs. However, higher SSTs do not guarantee that all TCs will become more intense. A warmer world may have more wind shear in the atmosphere and wind shear disrupts the structure of TCs to prevent intensification and can cause weakening in TCs (Vecchi & Soden, 2007). Furthermore, the increased atmospheric stability from more warming of the upper atmosphere compared to the lower atmosphere can inhibit the intensity of TCs due to suppression of convection and can slow the intensification of TCs due to global warming (Fu et al., 2011)(Tuleya et al., 2016). Mid-level atmospheric moisture also will likely change due to warming in the atmosphere, which will impact the intensity of TCs. Significant uncertainty exists concerning the global frequency of very intense storms and the global frequency of TCs in general does not seem to change despite higher SSTs (Landsea et al., 2010).

Following the Clausius-Clapeyron relationship, every 1 K warming results in an increase of 7% in the saturation water vapor content in the atmosphere (Held & Soden, 2006). More water vapor content in the atmosphere means increased potential for extreme precipitation, which is often the simplest explanation for why precipitation increases with warming (O'Gorman, 2015). O'Gorman, 2015 explains that other factors like dynamics and precipitation efficiency have also been linked to the changes in precipitation extremes. There has been research that tries to assign the contribution of different factors to the increase in precipitation in TCs (Wang et al., 2015). While an increase in SSTs does lead to more precipitation for TCs, the doubling of carbon dioxide with no warming has been shown to lead to little change in TC precipitation (Scoccimarro et al., 2014). For a +2K global warming, the mean change in the near storm precipitation rates of TCs is about 14%, with studies ranging from 6% to 22% (Knutson et al., 2020). Under a

+2K global warming case the tropical ocean is likely to be warming less than the global average, therefore the precipitation rate changes may end up being slightly stronger than the 7% increase in water content, sometimes termed "super Clausius-Clapeyron scaling". (Knutson et al., 2020).

TC size is important in helping determine impacts from wind and storm surge. Larger sizes are correlated to more economic damage done by the TC (Needham & Keim, 2014)(Zhai & Jiang, 2014). TC size does not appear to change much if at all (Wehner, 2021) with warming, although different basins might have different signals for size (Knutson et al., 2015) and other TC properties (Knutson et al., 2020). One problem is the lack of consistency in defining the TC size. Often the wind field is used to generate a metric as a proxy for size. Intense TCs tend to have metrics that can measure the wind field that is above the hurricane-force wind, usually 33 m/s and above. Some have used weaker winds to determine the size, usually a number much less than 17 m/s, which would be the minimum tropical storm force winds. For example, the radius of 12 m/s winds was used in (Knutson et al., 2015). Schenkel et al., 2017 suggested a radius of 6-10 m/s winds based on the evaluation of reanalysis data to QuikSCAT data. It is also suggested that relative humidity may play a role in controlling the size of TCs (Hill & Lackmann, 2009) due to the presence of rainbands that can help expand the TC wind field. Despite the different metrics used to show size, the current consensus is that TC sizes do not appear to change much under warming.

In terms of intensity, minimum sea level pressure (MSLP) decreases and maximum surface wind speed increases with warming. For maximum surface wind speed, the median and mean increases are roughly 5%, with a range between 1% to 10% increase (Knutson et al., 2020). The confidence of such an increase is higher among relatively high-resolution models of 60 km or smaller (Roberts, Camp, Seddon, Vidale, Hodges, Vannière, et al., 2020). Hill and Lackmann, 2011 found a larger central pressure deficit for both their 6 km and 2 km models, with the 2 km having a larger increase than the 6 km. Other studies have found a large decrease in the central pressure deficit while looking at different scenarios such as very intense TCs (Kanada et al., 2013).

1.3 Modeling of TCs

Modeling TCs has always been a challenge given the tension between accurately depicting TCs in global climate models (GCMs) and the computational costs of running models at smaller grid spacings as well as the need to run ensemble members. One

solution to bridge this tension is to run regional models that focus on a region while taking into account the environmental conditions that come from global models (Camargo & Wing, 2016). GCMs themselves are often run with resolutions of 100 km and are used to study the global aspects of TCs such as frequency, but will underrepresent intense TCs, due to their coarse spatial grids being unable to depict TC characteristics well (Eyring et al., 2016). Dynamical downscaling, which applies boundary conditions from the GCMs onto the regional model boundaries, can take advantage of the finer spatial resolutions while focusing on a specific region. Regional models can cover specific basins which makes it easier to determine what aspects of TCs are changing in that basin. At a resolution of 25 km, global climate models can closely simulate tropical cyclone frequency, spatial distribution, and intensity that are close to observations (Roberts, Camp, Seddon, Vidale, Hodges, Vanniere, et al., 2020). However, it has been pointed out that spatial resolutions larger than 25 km are not adequate in representing the intensities of very intense TCs in categories 4 and 5 of the Saffir-Simpson Scale (C. Davis, 2018). This makes sense when thinking about how some aspects of TCs such as simulating convection or eyewalls in intense TCs require much finer spatial resolutions and lead to models with coarser resolution underestimating intensities. Regional models have moved to a few kilometers in grid spacing, which allows for the depiction of convection without the use of parameterization, although there is a range from 10 km down to 100 meters that is regarded as a gray zone when considering an explicit treatment of convection (Tomassini et al., 2023).

1.4 Pseudo-global warming

Pseudo-global warming (PGW), also known as thermodynamic global warming, surrogate global warming, and imposed global warming, is a method to get information from GCMs to understand future climate conditions. Schär et al., 1996 introduced the methodology of PGW by leveraging regional climate models to see how precipitation in Europe changes with +2K warming given that GCMs had high spatial resolution. Now, PGW is used to first reproduce previous weather events and then applies the thermodynamic signal and reforecasts those same events in a warmer climate. The thermodynamic signal is derived from the temperature changes and other thermodynamic changes that come from GCMs (Rasmussen et al., 2011). Regional climate models are very important tools in PGW to downscale large-scale conditions to smaller scales.

A simple workflow of PGW simulations is as follows: To reproduce previous weather

events, one would need to use re-analysis data, which is obtained by assimilating weather observations into models to produce the best replication of past weather events (Hersbach et al., 2020). This re-analysis data is then downscaled to the regional level, where the regional models will run to replicate the historical weather events. After these are completed, the thermodynamic signal can be used to modify the re-analysis data. Then these now modified fields can be used to downscale the atmosphere to regional scales to get a new model run in a warmer climate.

One potential drawback of the PGW approach is that the climatology of the weather events is held the same. That is, a key assumption for PGW is that we hold the internal climate variability is held constant for the period of the historical weather events. Thus the changes in the frequency of these weather events are not quantified by the PGW approach. If the weather event does not occur at a certain location in the historical record, it is unlikely to hit that certain location in the future PGW simulation. Given those frequencies of weather events are not likely to be held constant in warmer climates, PGW is not a method that can be used to analyze frequency. It means any changes that do occur to TCs due to applying PGW come from the changes that are applied by PGW such as SSTs and other thermodynamic variables.

1.5 Studies with PGW and TCs

There have been studies that analyzed specific storms and how PGW affects the TCs in models. Patricola and Wehner, 2018 ran a 4.5 km resolution Weather Research and Forecasting (WRF) model using the Representative Concentration Pathways (RCP) scenarios of RCP4.5, RCP6.0, and RCP8.5 with convection-permitting to better quantify rainfall in tropical cyclones with future warming. They also quantified how the existing warming has impacted precipitation compared to a pre-industrial baseline. Using the RCP8.5 scenario, Hurricanes Katrina, Irma, and Maria have enhanced average precipitation in the RCP8.5 scenario compared to the historical scenario (Patricola & Wehner, 2018). The spatial pattern for precipitation changes is that the inner core gets wetter, but some areas outside of the TC have less precipitation. Furthermore, average precipitation increased as one went from RCP4.5 to RCP6.0 to RCP8.5, which corresponds to more warming. Both wind speed and rainfall were enhanced in 11 out of 13 intense TCs from around the world. There is more confidence in the projected TC changes in precipitation because the model was able to run with convection-permitting schemes, rather than using convective parameterization.

Gutmann et al., 2018 analyzed storms that pass through a domain of the East Coast and Gulf Coast of the United States. A 4-km WRF model was run to simulate TCs that impacted the United States between 2001 and 2013 with PGW warmings ranging from +3 to +6 K, although SSTs were warmed by +3.2 K from July to October. They identified 22 tracks that were analyzed out of 30 storms that were tracked within the domain (Gutmann et al., 2018). From this 13-year WRF simulation of historical and PGW cases, the mean maximum wind speed seemed to increase from 32 m/s to 34 m/s which was statistically significant. The average maximum rainfall rates increased by 24% from 83 mm/hr to 103 mm/hr. The MSLP decreased from 966 hPa to 962 hPa on average. Finally, it appears that the change in the radius of hurricane-force winds (over 33 m/s) is minimal and not statistically significant, which suggests the size of the hurricane-force winds does not change. These results agree with the established research done on TC changes due to climate changes and the 13-year period analyzed represented the longest duration PGW study in literature at the time.

Delfino et al., 2023 analyzed whether or not convective parameterization affects the results for PGW changes as well as how much warming that has already happened affected TCs. Delfino et al., 2023 used a 5 km version of WRF with a convective parameterization and a 3 km version of WRF without a convective parameterization and used the far-future SSP585 scenario as the baseline warming for the PGW. They simulated three intense typhoons, Bopha (2012), Haiyan (2013), and Mangkhut (2018), that impacted the Philippines. Maximum wind speed was found to increase in all three TCs and each of the two model runs. Meanwhile, the size of TCs seems to change relatively little and ranges between -7% to 12 % depending on the TC and model run. The biggest difference between convective parameterization and convection-permitting model runs was that they showed differing results for translation speed, with the 5 km run having faster translation speed, and the 3 km run having slower translation speed, both compared to present-day simulations.

Furthermore, Lackmann, 2015 and Nakamura et al., 2016 studied Hurricane Sandy (2012) and Typhoon Haiyan (2013), respectively, and provide good insight as to some of the particular changes that occur when applying PGW. Lackmann, 2015 looked at pre-industrial, current, and 2100 Sandy at the point at which it was near the Bahamas. From that point on, Lackmann, 2015 showed that applying PGW can impact Sandy's track and strength. The 2100 version of Sandy was stronger and made landfall on Long Island, while the pre-industrial version of Sandy was weaker and made landfall on the Delmarva peninsula. Meanwhile, Nakamura et al., 2016 showed that increasing SST

only would result in a decrease in MSLP of 21 hPa and a large increase in storm surge, while increasing SST, atmospheric air temperature and relative humidity only strengthen Haiyan by 13 hPa and a smaller increase in storm surge. This suggests that increasing SSTs only makes TCs stronger in PGW scenarios, while also increasing atmospheric air temperature and relative humidity helps moderate the increase in intensity.

One of the similarities that all PGW studies seem to share is the relatively small sample size used to analyze TCs. Most analyses focus on intense TCs, which is reasonable as they make the most impact and would be relatively easy to analyze compared to weaker storms. However, this means that they are implicitly biasing any generalized results towards these stronger systems since weaker TCs might behave differently than these intense storms.

Unlike the previous studies of PGW on TCs, our study will include a far larger sample of TCs and a more direct comparison of the same TC in the historical scenario and their warm counterparts. The TCs we chose to analyze include all observed TCs as long as the TC remains in our dataset after a trajectory cleaning process. It means that unlike previous studies we do not neglect weaker TCs, which end up making up the majority of our data. This means we are not basing our studies on more intense TCs, although we do include analysis on stronger TCs based on the pressure. It makes sense to have weak TCs, as impacts from weak TCs can still bring massive damage. We hypothesize that given a warmer climate, we expect more precipitation and more precipitable water due to more water vapor being present in our atmosphere. We should expect TCs to be more intense, although probably an increase smaller than our moisture variables because of higher SSTs. Finally, size should not change much because the relative moisture changes are minor. Looking at the TC characteristics including TC properties like intensity and moisture content and distribution of these properties across the historical and four warm scenarios will show the changes in TCs due to warming.

Chapter 2
Material and Methods

2.1 WRF Model

The simulations analyzed here were generated with a 12-km resolution version of the WRF model (Skamarock et al., 2021). Simulations were performed by researchers at Lawrence Berkeley National Laboratory using 1979-2019 ERA5 boundary conditions applied every 6 hours. The model configuration is fully described in Jones et al., 2023. Briefly, the configuration used to run WRF includes Thompson microphysics, Tiedtke cumulus parameterization, RRTMG for longwave and shortwave radiation, MYJ for the planetary boundary layer, Eta similarity for the surface layer, and the Noah Land Surface Model for the land surface. Readers are referred to the references above for more details.

The domain is centered over the contiguous United States (CONUS). It has 425 x 300 grid points and ranges from 21°N to 56°N in latitude, while longitude varies from 120°W to 73°W at the southern edge of the domain to 134°W to 60°W at the northern edge. Figure 2.1 shows the native domain of the model using the sea level pressure field for Hurricane Sandy as it approaches landfall.

A historical run from 1979-2019 serves as our benchmark case. Four future warming scenarios were performed over two different time periods, 2019-2059 and 2059-2099, although the meteorology from these periods is the same as the benchmark case – in other words, the same large-scale meteorology is recreated for two additional future time periods. In these time periods, thermodynamic global warming is applied. Two Shared Socioeconomic Pathways (SSP) scenarios were run by Jones et al., 2023. One is SSP245, in which SSP2 is the middle-of-the-road scenario that extrapolates past and current development into the future and has an additional global radiative forcing of 4.5 W/m^2 by 2100. The other scenario is SSP585, where SSP5 is a fossil fuel-dependent scenario with an additional global radiative forcing of 8.5 W/m^2 by 2100. SSP scenarios

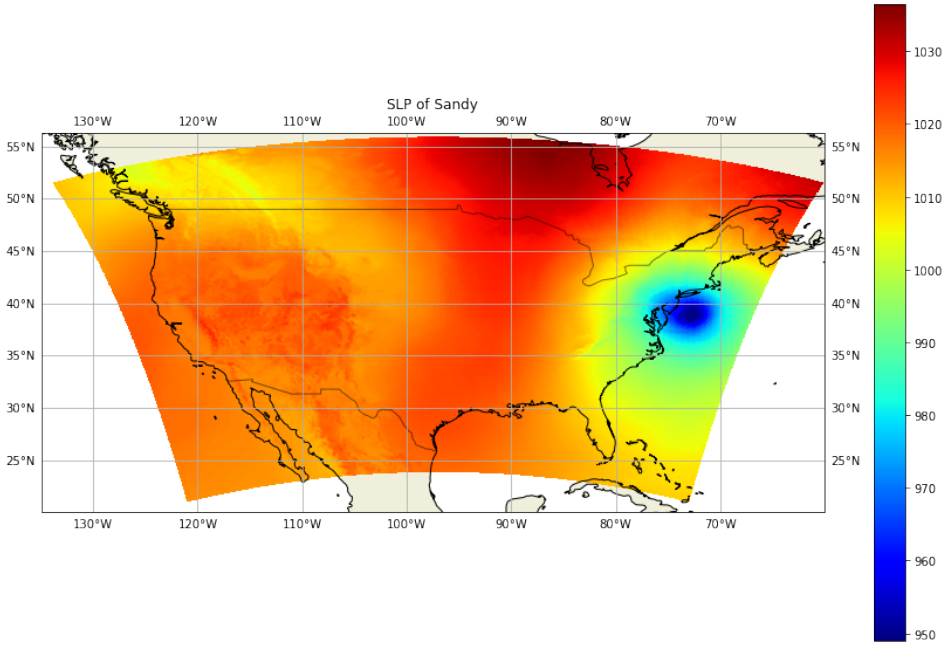

Figure 2.1: WRF output of Hurricane Sandy at 21Z October 29th, 2012 of sea level pressure. The domain of the model covers CONUS and much of Canada and Northern Mexico. It also contains parts of the Eastern Pacific and North Atlantic basins.

are new future scenarios that factor in different socio-economic developments as well as the previous RCP scenarios that have been incorporated into Earth system models like the 6th climate model intercomparison project (CMIP6) (Riahi et al., 2017). At the time of this project, the SSP245 model data had not been fully generated, so the warm scenario we focus on is from the SSP585 runs only.

The warming scenarios that are modeled are the low and high-sensitivity models for SSP585. In climate science, climate sensitivity is the responsiveness of the increase in temperature due to the increase in greenhouse gases like carbon dioxide. Given the same climate forcing, a low sensitivity means less warming, while a high sensitivity means more warming. The 2019-2059 time period is called 'near,' and the 2059-2099 time period is called 'far.' Furthermore, there are 'cold' versus 'hot' in the near and far scenarios. They denote a spread in models of the warming due to climate sensitivity. The 'cold' scenarios represent the 4 ensemble models that had low climate sensitivity, whereas 'hot' represents the 4 ensemble models that had high climate sensitivity. We, therefore, refer to these simulations as 'cold-near,' 'hot-far,' etc.

Jones et al., 2023 applied CONUS warming to the 40 years of historical data and then used time-evolving thermodynamic climate signals that are applied to each year

to show a future warming trajectory. The 40-year runs are not continuous due to the discontinuity at the boundaries of 2019 to 2020 and 2059 to 2060, thus we analyze blocks of 40-year periods. For reference, the year 2000 in the historical period, corresponds to 2040 in the near time period, and 2080 in the far time. A TC that occurred in 2000 can also be found in the data for the warm scenarios in 2040 and 2080.

As with previous PGW simulations, the thermodynamic environment is changed, but more specifically, air temperature, near-surface air temperature, skin temperature, relative humidity, and SSTs are updated in the warming runs. The ERA5 boundary conditions at the domain's edge as well as the SST boundary conditions are changed using the PGW approach and thus the four warm scenarios are generated from that. Jones et al., 2023 also note that they calculate these signals from monthly data and that these signals are evolving, so the temperature is also changing with respect to time. The general order from coolest to warmest (based on CONUS-mean surface temperature) for the warm scenarios is 'cold near,' 'hot near,' 'cold far,' and 'hot far.' The WRF data for the historical and the two SSP585 warm scenarios is publicly available and can be accessed online (Jones et al., 2023).

2.2 TempestExtremes

TempestExtremes (TE) is a software package developed by (Ullrich & Zarzycki, 2017) that is used to track TCs in gridded climate data. The International Best Track Archive for Climate Stewardship (IBTrACS) is a database of all recorded TCs in the world created and maintained by Knapp et al., 2010 and can be accessed here (Knapp et al., 2018). For the basins surrounding CONUS, this data primarily comes from the National Hurricane Center. IBTrACS and TE were used together to generate trajectory files for storms in the model. We first use DetectNodes and StitchNodes to identify potential TCs. Furthermore, TE has further applications by taking snapshots of TCs at time steps from the model as well as creating an average of all the snapshots found by TE using the NodeFileFilter and NodeFileCompose algorithms (Ullrich et al., 2021).

2.3 Trajectory Files

Since there is no guarantee that a storm follows the exact track from IBTrACS, we apply a special tracking methodology to the PGW runs. We first mask the sea level pressure (SLP), only retaining grid cells if they are within 3° of a historical TC at a

given time snapshot as defined by IBTrACS. Then, we track SLP on this masked field, seeking all local minima, which are defined by a value completely enclosed by values higher than it. Next, we merge any SLP minima within 4° of one another at a given snapshot keeping the lowest value. This is to ensure that we are keeping the minimum SLP location associated with a given historical storm, but allowing for the storm centers to deviate from the exact SLP as reported in IBTrACS. Storms are then stitched together in time and meet the two criteria of persisting for at least 12 hours or 3 timesteps and traveling no more than 5° in any given 6-hourly timestep. Otherwise, the two snapshots are considered two distinct trajectories.

However, there is no guarantee each track file exactly matches. For example, weaker TCs may get broken into multiple tracks in the future warm runs when they weren't in the historical runs. Certain storms may be able to be tracked for an additional timestep or two. Before any analysis of the historical and four warm scenarios, the data in each of the five scenarios needed to be free of such inconsistencies, as well as each line of each trajectory was required to match the same storm in all five scenarios. This was done by analyzing the contents of the trajectory files and by matching them with the IBTrACS database to make sure that a TC existed and corresponded to a trajectory. If a TC is not present in any of the historical and four warming scenarios, that TC is ignored and deleted from the trajectory file. Some TCs might represent two or three trajectories, which means choosing the trajectory that best represents that TC while analyzing the other trajectories to see if it makes sense to combine trajectories. We also made sure that such TCs were indeed present in the historical record by being in the database of IBTrACS.

Afterward, each trajectory was checked to have the same amount of time steps and lasted in the same period, so that comparisons can be done for a TC in each scenario. Figure 2.2 shows the steps that were followed in what we refer to as the 'cleaning process.' The final result is five trajectory files each containing the same storms and the exact time relative times in all five simulations. This allows us to compare the exact same storm at the exact same timestep across all model runs. With the corrected trajectory files, TE's NodeFileFilter and NodeFileCompose were used to take snapshots and create composites of snapshots. In the end, 346 individual TCs were found between 1979-2019 in both the Northern Atlantic and Eastern Pacific regions in the domain with 4,498 total snapshots, which are time steps of a given TC, among them.

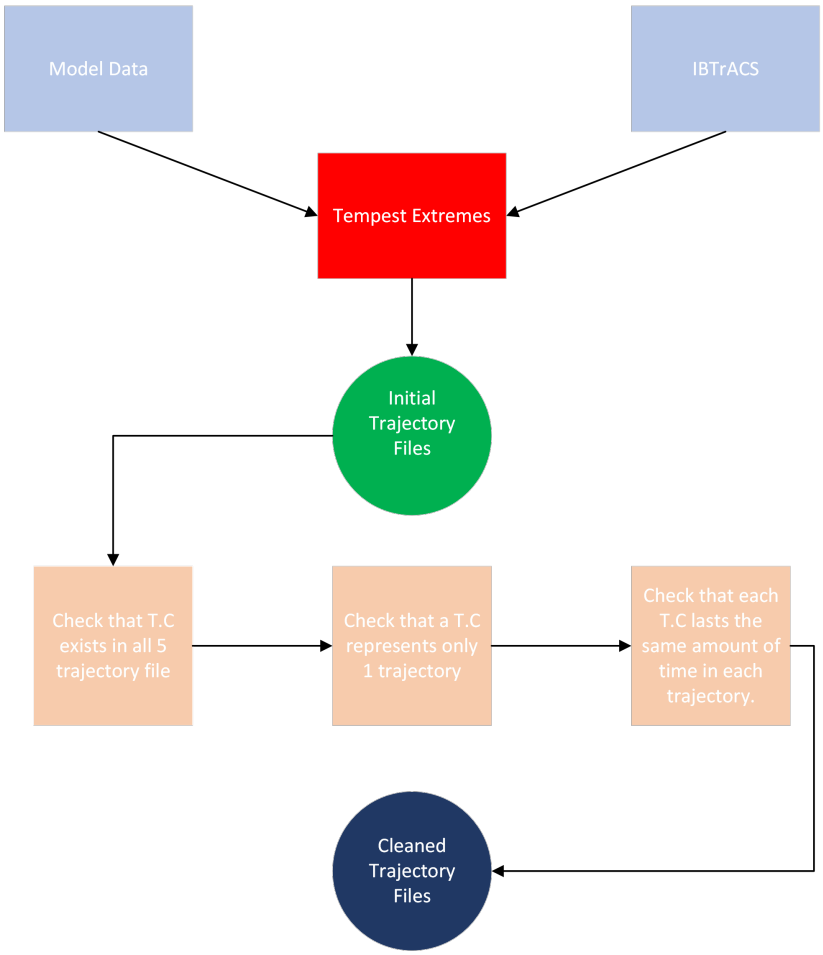

Figure 2.2: A flow chart that shows the steps in processing the trajectory files to have better comparisons between the historical case and the four warm scenarios.

2.4 Data Analysis

Taking composites of the various amounts of data of the TC is taking an average of all the snapshots, thus first we will show the composites of variables of the TC. TC intensity is measured by the minimum sea level pressure (MSLP) and maximum winds. For our purposes, TC intensity was chosen to be the MSLP as the data for pressure was more consistent than maximum winds. Four bins were created to separate TCs into weak, medium, strong, and very strong intensities. The weak intensity bin was denoted as TCs having more than 1000 hPa and contains 2,966 snapshots. The medium-intensity TCs range from 980 hPa to 1000 hPa and include 1,106 snapshots. The strong intensity defined TCs that range from 965 hPa to 980 hPa; 271 snapshots lie in this bin. Finally, the strongest intensity was TCs that had less than 965 hPa with 155 snapshots. This

binning can considered to be analogous to analyzing weak tropical storms, strong tropical storms, Category 1-3 TCs, and Category 3 and higher TCs (Service, 2019). Analysis of the data consisted of taking the differences between the four warming scenarios and the historical scenario to see how different TC characteristics changed over warming. The TC characteristics that were analyzed included surface winds, 850 hPa winds, precipitation, precipitable water (TMQ), MSLP, areas of winds and precipitation, size of the TC, as well as the radius of maximum winds. It was noted earlier that TC size is not a particularly well-defined metric. In our analysis, we will define the TC as the 850 hPa winds that exceed 8 m/s because it has been shown to represent the wind field of a TC in gridded data (Schenkel et al., 2017). Note that 850 hPa winds were chosen to limit the impact of friction from the surface on the values of wind, these winds are approximately 15% higher in magnitude than the surface winds.

2.5 Comparing TE-derived path with IBTrACS

Figure 2.3 shows the path of Hurricane David (1979) determined by TE compared to IBTrACS. The trajectory that was derived using TE is close to the observed path from IBTrACS through the entire WRF domain. TE was able to track Hurricane David, which was a well-defined, intense TC because its minimum pressure was low enough that WRF could differentiate it from the background pressure field. However, for weaker storms with higher minimum pressure, such as Tropical Storm Allison in 2001, WRF produced a TE track that had substantial differences compared to IBTrACS as seen in Figure 2.4. Despite such differences, the TE-derived track generally followed the IBTrACS track and the inclusion of IBTrACS helps in making the search of such TC in the model data.

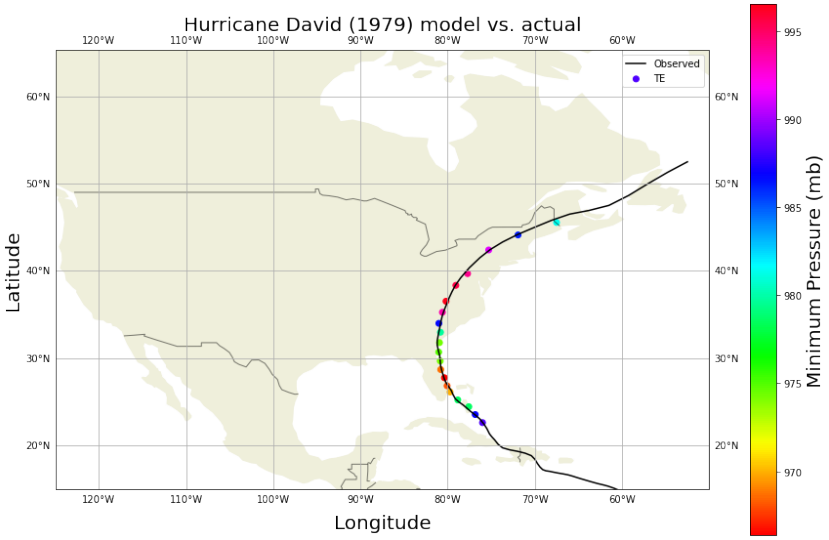

Figure 2.3: Comparing TE and IBTrACS location of Hurricane David (1979). The black line represents the entire path of Hurricane David from IBTrACS, while the individual dots represent Hurricane David as tracked by TE color-coded by minimum sea level pressure.

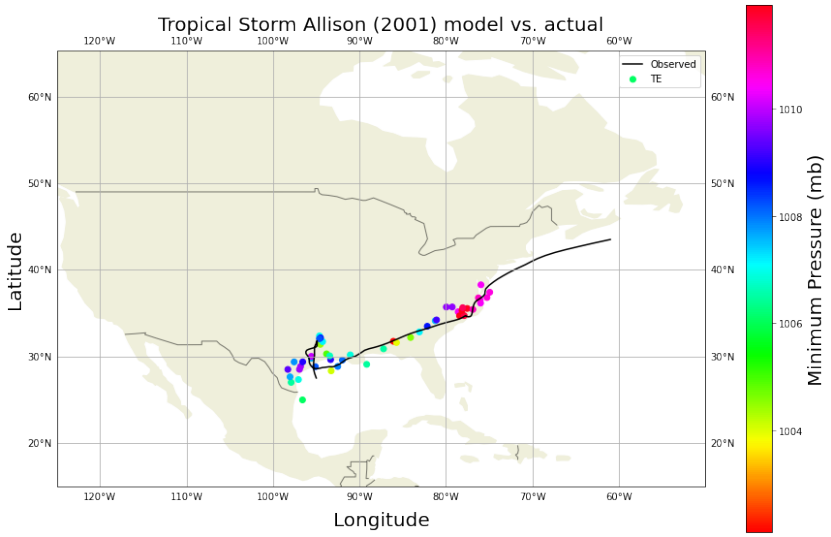

Figure 2.4: Same as Figure 2.3, except plotting Tropical Storm Allison (2001).

2.6 Compare historical and PGW trajectories

Comparisons of the track of a TC in both the historical and the four warming scenarios are needed. Given that applying the same ERA5 boundary conditions should mean the meteorological record should be replicated in all five datasets. Figure 2.5 gives us a look at Hurricane Sandy (2012) and shows that the track of the storm is similar in all five datasets. The results of the trajectory files being cleaned show that the tracks generally last the same distance and there are small deviations of the tracks for each scenario.

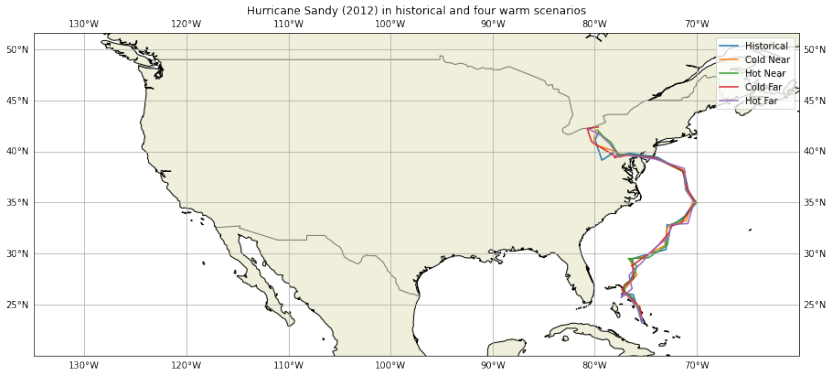

Figure 2.5: Plots the track of Hurricane Sandy (2012) from the historical and four warm scenarios.

Chapter 3
Results

3.1 How do TCs change with different warming scenarios?

Figures 3.1 to 3.5 all follow the same format. On the left is a composite plot of all TCs in the historical simulation, which plots the values of a given TC quantity. The four-panel plots on the right are the difference between the four warm scenarios and the historical scenario. Thus the four-panel plots give us the change in these TC quantities in the four warm scenarios. The black contour line is the 8 m/s 850 hPa winds that were defined as the size of the TC and 12 m/s 850 hPa winds is the yellow contour line.

Looking at the historical plot, we see that precipitable water (TMQ) is a quantity that increases as we get closer to the TC center. A slight asymmetry to the right side of the TC is noted. For TMQ, the changes to them in the warmer scenarios are all increasing. In Figure 3.1, TMQ is increasing in all spatial directions. This is noticeable with increases in TMQ seen even outside of the 8 m/s contour line in black and the 12 m/s yellow contour line, although the TMQ increases in the center of TCs are higher. The increase in TMQ towards the center of the TC is greater in the 'cold far' and 'hot far' scenarios, whereas the 'cold near' and 'hot near' scenarios look more uniform in the increase of TMQ spatially. It is clear that the increases in these variables are ordered from smallest to largest in the order of least to most warming. 'Cold near' is the smallest increase in TMQ, while 'hot far' has the largest increase in TMQ.

For Figure 3.2, the historical plot has the highest values of precipitation confined to the northeast of the center of the TC, which happens to be a relatively drier part of the TC due to it being the TC center which can have an eye that would preclude precipitation and clouds. For the four warming scenarios, precipitation is also increasing similar to TMQ, but the increase is more confined to the TC center. The precipitation increase was concentrated near the center of the storm in all four warm scenarios as

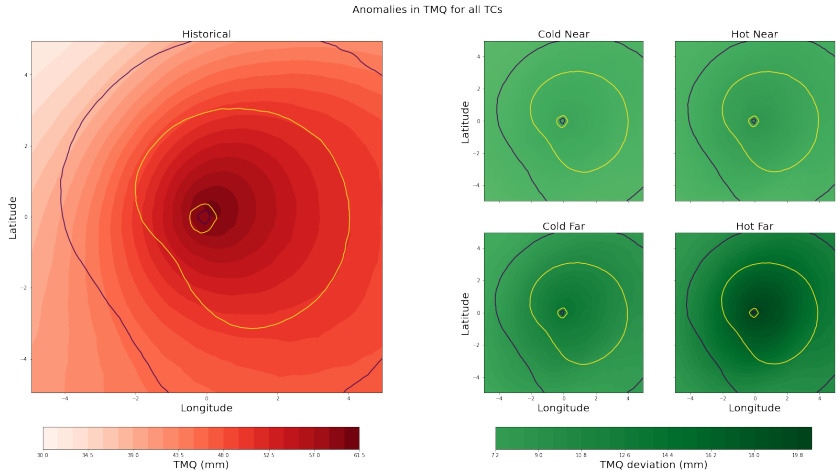

Figure 3.1: On the left is the historical average precipitable water for all TCs. On the right is a four-panel plot of 4 warming scenarios that show how the composite precipitable water changes. The black contour line is the 8 m/s 850 hPa winds and the 12 m/s 850 hPa winds is the yellow contour line.

seen with it being confined to inside the yellow contour line of 12 m/s. The cooler warm scenarios of 'cold near' and 'hot near' have precipitation increases that are smaller and a bit more uniform in the TC core. Higher increases in precipitation can be seen to the north of the TC center in the plot of the 'hot far' scenario as well as the 'cold far' scenario. The precipitation change outside of the TC appears to be very minimal, with slight decreases or increases found. It shows that although both TMQ and precipitation do increase, the increase in TMQ is much more widespread spatially.

In Figure 3.3, the SLP is plotted along with the changes in SLP in the four warming scenarios. In the historical plot of SLP, we see that the lowest values of SLP are found in the center of the TC and the difference in SLP is highest close to the MSLP. For the changes in SLP in the warm scenarios, the SLP becomes lower, especially in the center of the TC. Also, note that the warmer scenarios had a greater decrease in SLP at the center of TC. The decrease in pressure is not seen elsewhere in the TC, whether you use the 8 m/s line or the 12 m/s line. Otherwise, the SLP appears to increase outside of the center of the TC, which means the warm scenarios feature a larger SLP differential between the TC and its environment. It would mean higher magnitude winds for the TC in the warm scenarios due to increased pressure gradient force.

Figure 3.4 shows the historical surface winds as well as the changes in surface winds in the warming scenarios, while Figure 3.5, shows 850 hPa historical winds and changes in 850 hPa winds. Both have increases in winds, which makes sense given the changes in

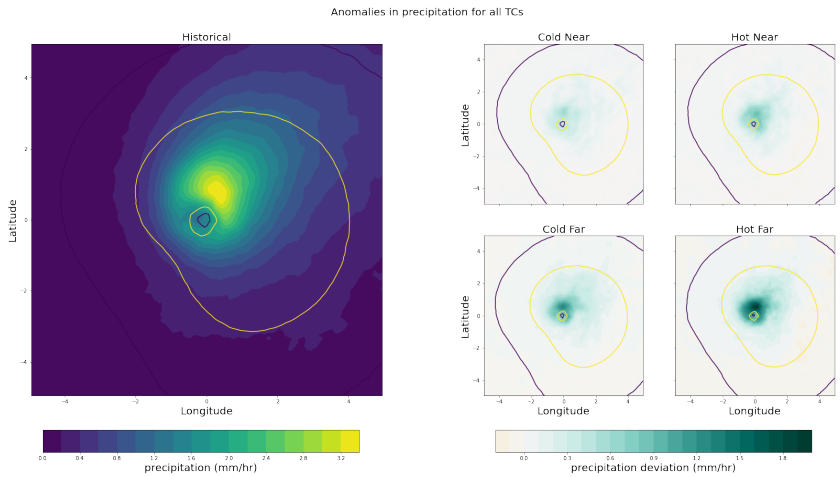

Figure 3.2: On the left is the historical average precipitation for all TCs. On the right is a four-panel plot of 4 warming scenarios that show how the composite precipitation changes. The black contour line is the 8 m/s 850 hPa winds that were defined as the size of the TC and 12 m/s 850 hPa winds is the yellow contour line.

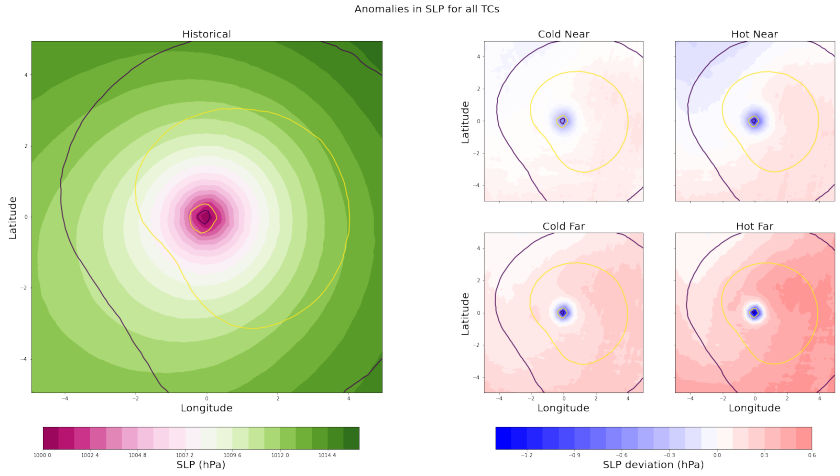

Figure 3.3: On the left is the historical average MSLP for all TCs. On the right is a four-panel plot of 4 warming scenarios that show how the composite MSLP changes. The black contour line is the 8 m/s 850 hPa winds and the 12 m/s 850 hPa winds is the yellow contour line.

SLP discussed above. Once again, like in Figure 3.3, the wind increases are confined to the center of the TC, and such increases are only a fraction of the area bounded by the 8 m/s contour line or the 12 m/s contour line. Interestingly, the 850 hPa historical winds have a dipole structure in that the highest 850 hPa winds do not surround the center of the TC. This might suggest a tilting in the vertical structure in the composite TC or since we didn't take into account the motion of the TC, it could be the translation

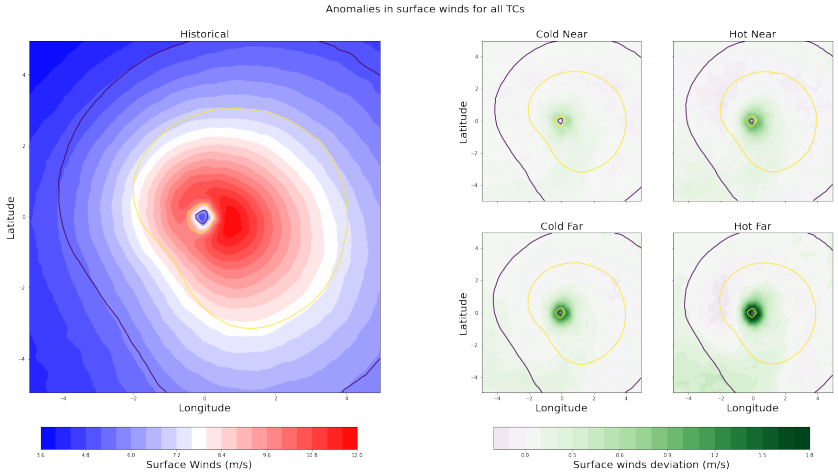

Figure 3.4: On the left is the historical average surface wind field for all TCs. On the right is a four-panel plot of 4 warming scenarios that show how the composite surface winds change. The black contour line is the 8 m/s 850 hPa winds and the 12 m/s 850 hPa winds is the yellow contour line.

vector causing this tilt. The surface winds are less lopsided in the area where the fastest winds are. This has been seen in observed TCs in which environmental wind shear has played a role in the asymmetry of TC structure (DeHart et al., 2014).

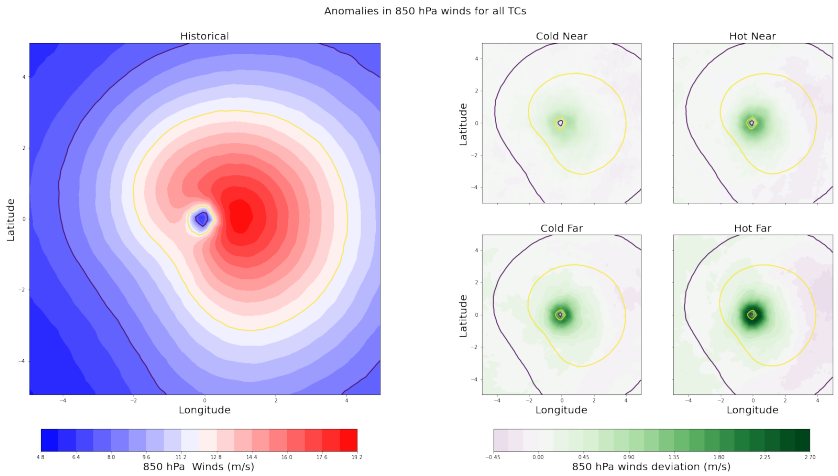

Figure 3.5: On the left is the historical average 850 hPa winds for all TCs. On the right is a four-panel plot of 4 warming scenarios that show how the composite 850 hPa winds changes. The black contour line is the 8 m/s 850 hPa winds and the 12 m/s 850 hPa winds is the yellow contour line.

3.2 General statistics

Statistics of certain TC properties					
Variable	Historical	Cold Near	Hot Near	Cold Far	Hot Far
Max TMQ (mm)	68.4	75.4	78	84.8	93
Max precipitation (mm/hr)	22.9	26	27.5	30.1	33.7
Max surface winds (m/s)	18.4	18.9	19.2	19.5	19.9
Max 850 hPa winds (m/s)	28.2	29.0	29.4	29.8	30.4
Min SLP (hPa)	1000.3	999.7	999.3	999.1	998.9
R8 radius (km)	469.7	471.2	469.1	468.4	468.6
10 mm/hr area (100 km^2)	73	88	94	107	118
Radius of max winds (km)	147.9	140.1	143.1	140.4	141

Table 3.1: Table of the values of TC properties in the historical case and the four warm scenarios for all TCs.

Table 3.1 shows some selected variables, which are calculated from all the snapshots and then averaged together. The average maximum (max) TMQ increases from 68.4 mm in the historical to 93 mm in the 'hot far' scenario. Maximum TMQ shows a monotonic increase in TMQ as temperature increases. We can also see that the percent changes are large, Maximum TMQ increased from 10.2% from the historical value in the 'cold near' to a 36.0% increase in the 'hot far' case. Maximum precipitation also increases from 22.9 mm/hr in the historical to 33.7 mm/hr in the 'hot far' scenario. Maximum precipitation increases outpace the increases seen in maximum TMQ. Every warm scenario has a maximum precipitation increase by a greater percentage than the maximum TMQ, as seen in Figure 3.6. Maximum surface winds go from 18.4 m/s to 19.9 m/s and maximum 850 hPa winds go from 28.2 m/s to 30.4 m/s. Both maximum surface winds and maximum 850 hPa winds changed at a very similar rate in terms of percent change, as in each warming scenario, both wind variables had a percent increase that was within 0.2% of each other when looking at Figure 3.6. This makes sense, given winds are often dependent on the gradient of SLP between the environment and the MSLP. For MSLP, the values are getting lower, but the change is relatively small, at most a 0.1% decrease according to Figure 3.6 or about a 1-2 hPa decrease.

Next, we have R8, which is the radius at which 8 m/s at 850 hPa exists. It is a proxy for the size of the TC and any changes to the size in the future are small, with the 'cold near' seeing a small increase in the size, whereas the other warm scenarios see a small decrease in the size. 10 mm/hr area is a variable to show the area in which the TC is covered by 10 mm/hr or higher rainfall rates. It is clear that the area increases a lot with

warming, with increases ranging from 20.5% to 61.6%. This seems to further confirm the pattern that moisture-related variables are increasing at much higher magnitudes than other variables. Finally, the radius of maximum winds appears to show a decrease in the warm scenarios, although there is no real pattern to the decrease as the largest decrease comes from the 'cold near' scenario, while the smallest decrease comes from the 'hot near' scenario. It might suggest that the radius of maximum winds could decrease with warming, but there are a lot of factors to consider. All variables in each of the warm scenarios were compared to the historical and a p-value was calculated using a paired Student's t-test and all p-values were calculated to be $p < 0.01$. Therefore, while some of the aforementioned changes may be small, they may be statistically distinct due to the large, matched sample size of the data.

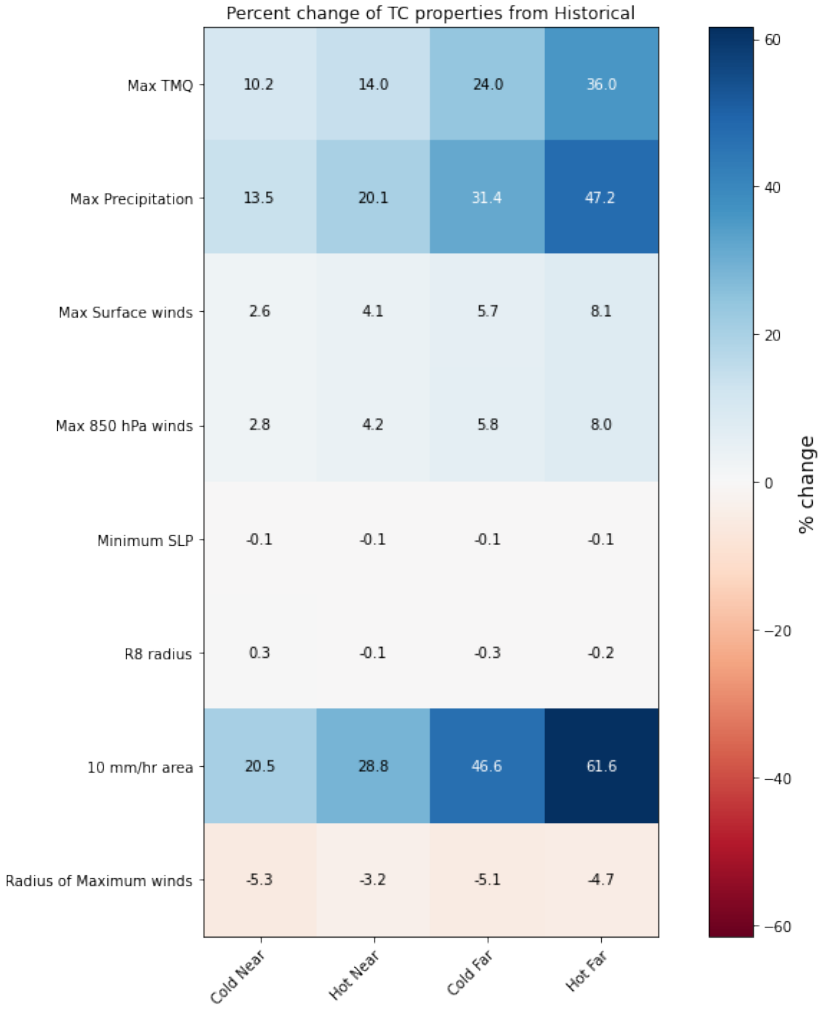

Figure 3.6: A heat map that shows the percent change of certain TC variables from the historical base to the four warm scenarios.

3.3 Does filtering by intensity matter?

We seek to check whether having a stronger intensity from the historical case affects the TC properties that are measured. This is done with the intensity bins that we have defined in section 2.4.

Statistics of Max TMQ via intensity					
Variable	Historical	Cold Near	Hot Near	Cold Far	Hot Far
> 1000 hPa	66.2 mm	72.8 mm	75.2 mm	81.9 mm	89.5 mm
		10.0 %	13.6 %	23.7 %	35.2 %
980-1000 hPa	70.6 mm	78.1 mm	81.1 mm	87.9 mm	97.1 mm
		10.6 %	14.9 %	24.5 %	37.5 %
965-980 hPa	77.0 mm	84.9 mm	88.1 mm	95.2 mm	105.3 mm
		10.3 %	14.4 %	23.6 %	36.8 %
<965 hPa	80.3 mm	88.1 mm	91.5 mm	99.1 mm	109.4 mm
		9.7 %	13.9 %	23.4 %	36.2 %

Table 3.2: Table of the values of average maximum TMQ in the historical case and the four warm scenarios for all TCs. Below each of the warm scenario values are the percent changes from the historical average maximum TMQ increase.

By separating snapshots by intensity, we can see that with maximum TMQ, the percent changes are all similar to each other no matter which intensity is used and which warm scenario is used. Looking at Table 3.2, we see that in the 'cold near' scenario, the average maximum TMQ increases from the historical in the range of 9.7-10.6 %. For the 'hot near' scenario, such changes range from 13.6-14.9%. 'Cold far' increases range from 23.4-24.5%. Finally, 'hot far' increases in a range from 35.2-37.5%. TMQ not being dependent on intensity is not a surprise given that TMQ is a measure of water content that depends on the temperature of the environment.

Despite TMQ increases being very similar no matter which intensity you use, for maximum precipitation, the intensity does seem to matter. In Table 3.3, the increases in precipitation are not the same for each intensity bin. The increase in maximum precipitation does appear to be greater than the change in maximum precipitation in Table 3.2. The changes in the strongest and weakest intensity bins are somewhat similar to each other, while the changes in the medium-weak and medium-strong intensities are also similar to each other. The separation between these two groups is evident from the least warmed scenario, the 'cold near.' We see that the increase in maximum precipitation for the 'cold near' case is 14.2-15.2% for the middle-intensity category, while the weakest and strongest intensity bins are an 11.9-12.5% increase. The divergence is

Statistics of Max precipitation via intensity (mm/hr)					
Variable	Historical	Cold Near	Hot Near	Cold Far	Hot Far
> 1000 hPa	20.2	22.6	23.9	25.4	28.1
		11.9 %	18.3 %	25.7 %	39.1 %
980-1000 hPa	26.3	30.3	32.4	37.2	42.2
		15.2 %	23.2 %	41.4 %	60.5 %
965-980 hPa	31.0	35.4	38.2	41.8	47.4
		14.2%	23.2%	34.8 %	52.9 %
<965 hPa	37.6	42.3	43.7	48.3	54.3
		12.5 %	16.2 %	28.5 %	44.4 %

Table 3.3: Table of the values of average max precipitation in the historical case and the four warm scenarios for all TCs. Below each of the warm scenario values are the percent changes from the historical that the average max precipitation changed in each warm scenario.

only more prevalent to the point where all the intensity bins are different from each other. Interestingly, the medium intensity bin of 980-1000 hPa TCs had the highest increase in maximum precipitation for all warm scenarios, while the weak intensity bin of >1000 hPa TCs had the smallest increase in maximum precipitation for all warm scenarios. For both maximum TMQ and maximum precipitation, a paired student's t-test was calculated and all variables were $p < 0.01$.

3.4 Distributions of TC-relevant quantities

In Figure 3.7, the distribution of maximum TMQ is shown from the historical and four warm scenarios. The distributions are very distinct and show the mode becoming less frequent while shifting the distribution towards higher values of TMQ. This is confirmed in Table 3.4, which shows that the 95th percentile of maximum TMQ does appear to increase more in terms of magnitude compared to the 5th percentile of maximum TMQ. The range of the maximum TMQ also increases as we go to increasingly warmer warm scenarios. The median is increasing, which is not surprising given the drastic difference in the distributions of maximum TMQ. Out of all the distributions of variables, this is the most stark change for any variable.

In Figure 3.8, the distribution of maximum precipitation peaks at 15-20 mm/hr rates, but the tail of the extreme precipitation rates gets longer and fatter as we go from the historical case to the four warm scenarios. This is shown further when looking at the extreme end of the precipitation rate. At the same time, we have some statistics in

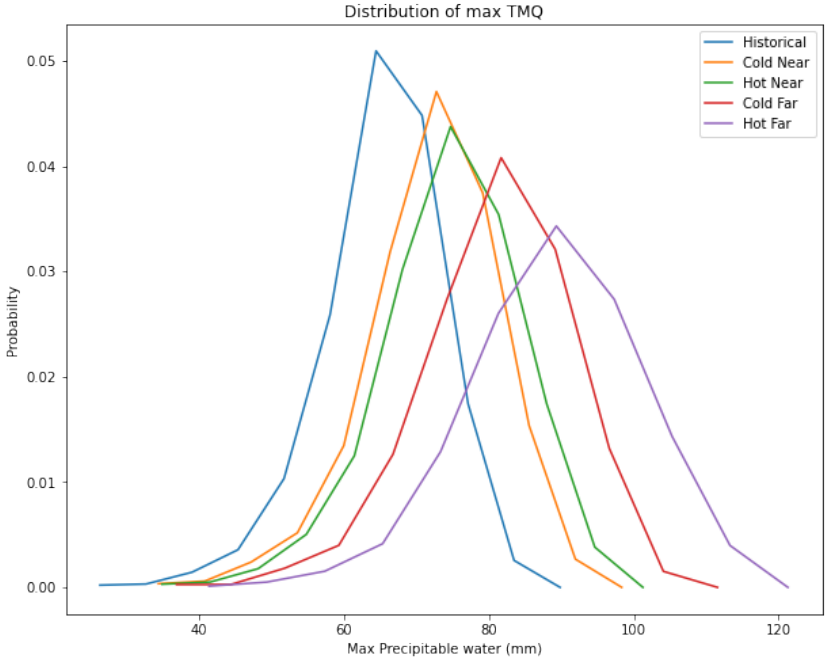

Figure 3.7: Distribution of Max TMQ

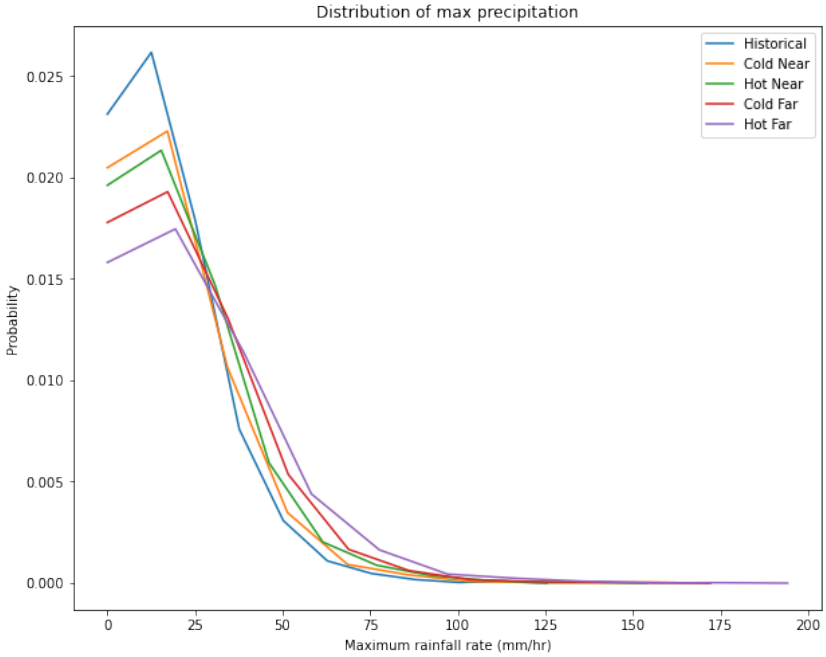

Figure 3.8: Distribution of Max Precipitation

Table 3.4, where the 5th percentile ranges from 2.3-2.9 mm/hr, and the 95th percentile increases from 52.6 mm/hr in the historical case to 76.1 mm/hr. The ranges of the distributions do increase compared to the historical, although 'hot near' has a smaller

range compared to the other warm scenarios. The median is also increasing, but we know that it is due to the increase in the higher-end maximum precipitation, rather than a systematic shift towards higher precipitation all around.

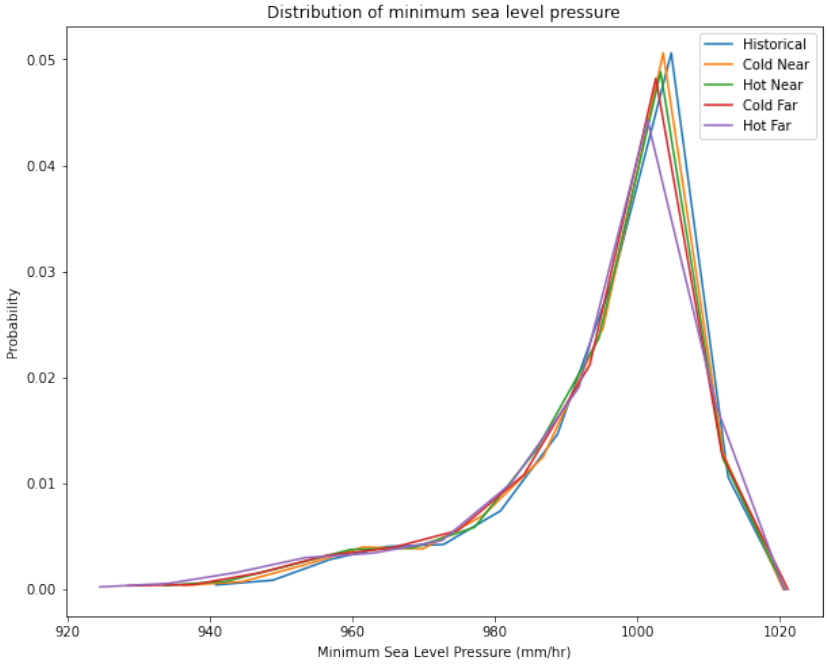

Figure 3.9: Distribution of MSLP

Figure 3.9 shows the distribution of the snapshots in terms of MSLP. MSLP appears to have a maximum peak of around 1005 hPa, which makes sense given most snapshots appear to be of tropical storm strength TCs. The interesting aspect is that the warmer distributions appear to have longer tails towards the smaller MSLP and that the mode is smaller and somewhat more intense. Furthermore, we see this with the stats that are given in Table 3.4, where the 5th percentile is the one that appears to decrease by a couple of hPa, whereas the 95th percentile is close to 1014 hPa. Furthermore, the median of the SLP does not seem to change all that much. The range does appear to change and confirms that the tail at the lower end of the SLP is increasing. For these three sets of distributions, the p-values for each warm scenario were calculated to be $p < 0.01$ using a paired Student's t-test.

Statistics of Max precipitation distribution					
Property	Historical	Cold Near	Hot Near	Cold Far	Hot Far
5th percentile	2.3	2.6	2.9	2.6	2.9
95th percentile	52.6	58.9	62.6	67.1	76.1
median	20.2	23.4	24.3	27.0	30.2
range	125.5	171.3	153.7	172.0	194.1
Statistics of Max TMQ distribution					
	Historical	Cold Near	Hot Near	Cold Far	Hot Far
5th percentile	53.6	59.4	61.4	67.1	73.3
95th percentile	80.8	89.1	92.5	100.2	111.4
median	69.1	75.9	78.5	85.5	93.4
range	63.5	64.0	66.4	74.7	79.9
Statistics of MSLP distribution					
	Historical	Cold Near	Hot Near	Cold Far	Hot Far
5th percentile	969.0	967.5	965.7	965.1	962.7
95th percentile	1013.8	1013.6	1013.7	1013.7	1014.0
median	1004.5	1004.5	1004.1	1004.1	1004.0
range	79.8	84.2	87.0	92.6	96.0

Table 3.4: Select stats on the distribution of Max precipitation, max TMQ, and MSLP.

3.5 Snapshot properties

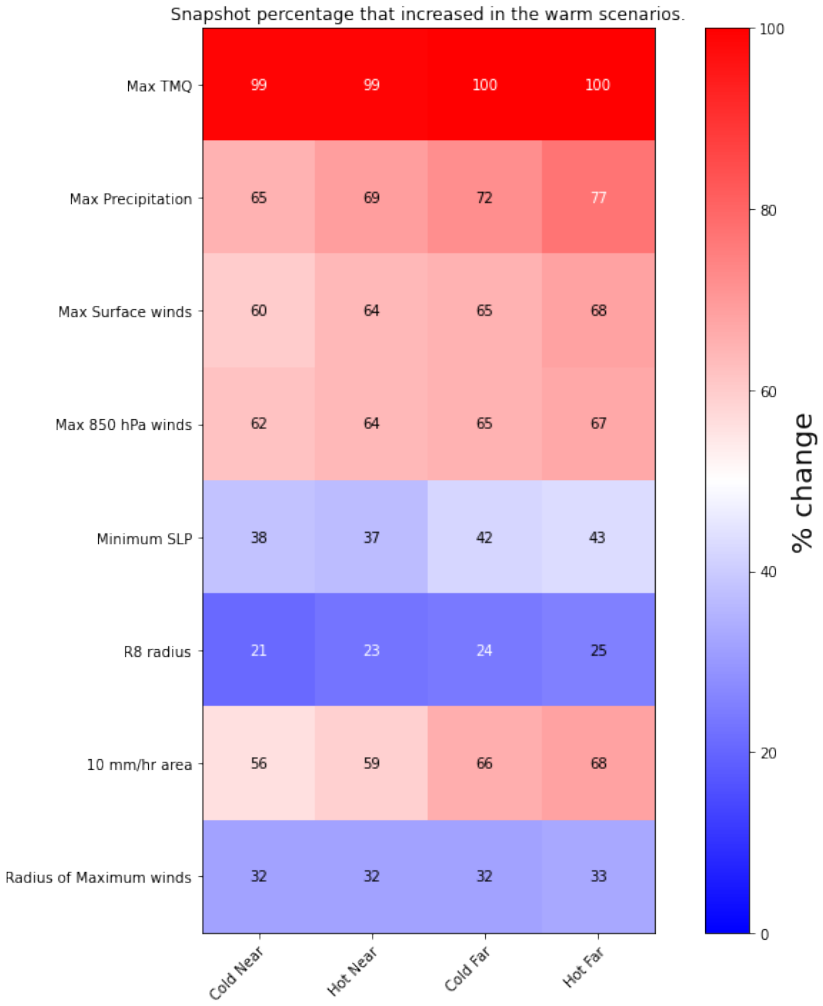

Figure 3.10: A heat map that shows the percentage of snapshots where the TC metric increased from the historical base to the four warm scenarios

Figure 3.10 shows the percentage of snapshots that increased in a specified variable at different warm scenarios compared to the historical. Maximum TMQ will almost always increase no matter which snapshot you choose to compare between any of the four warm scenarios and the historical, with 99 to 100 % of snapshots increasing from the historical case to any of the four warm scenarios. Maximum Precipitation ranges between 65-77% of snapshots increasing in magnitude from the historical scenario to the warm scenarios, which suggests more snapshots have increases in maximum precipitation, but some snapshots do have decreases in maximum precipitation when going from the historical to the four warm cases. The maximum precipitation snapshots have a higher

percentage of increasing when going from the 'cold near' to 'hot far' cases. There is also a 10 mm/hr area where the amount of snapshots that increase in area is much closer to 60%. Given the dramatic increase that was found in Figure 3.6, it might suggest that these increases are much higher compared to the decreases in area. However, it does appear that the warmer 'warm' scenarios have a higher percentage of snapshots that increase in the 10 mm/hr area.

For maximum surface and maximum 850 hPa winds, both have more snapshots increasing in magnitude from the historical to the warm scenarios, but the percentages range from 60 to 68 and 62 to 67 respectively. Also, the increases in the percent of snapshots increasing in value in the warmer scenarios are noted for both maximum wind variables.

Some variables like MSLP, R8 radius, and radius of maximum winds have more snapshots that decrease in magnitude than increase. For MSLP, 38-43% of snapshots increase in MSLP, which means 57% to 62% of snapshots decreased in MSLP. More snapshots decreasing in MSLP would be consistent with more intensification in a warmer world than not, but lots of differences in conditions that could increase or decrease MSLP. Size actually has the least amount of snapshots increasing in size, in which only 21-25% of snapshots increase in size compared to the historical case. That means 75% to 79% of snapshots decrease in the R8 radius metric. This is surprising given that R8 radius does not change much on average, this means that the snapshots that do increase in R8 radius on average have a bigger increase than the snapshots that decrease in R8 radius. Finally, the radius of maximum winds only increases in 32-33% of snapshots in all warm scenarios. That means the radius of maximum winds decreased in 67-68% of snapshots for the warm scenarios.

3.6 Rapid deepening and Rapid collapse events

One aspect that can be done with snapshot analysis is that we can check to see whether the amount of events defined by rapid deepening, a decrease of 10 hPa over 6 hours or lower, or rapid collapse, an increase of 10 hPa over 6 hours or higher, has changed.

There is a clear pattern in that there are more rapid collapse events than rapid deepening events. Both types of events are increasing in frequency as we go from the historical case to the warm scenarios. Also, note that these are still rare events in the snapshots that have pressure differences from previous snapshots. Although we have

4498 snapshots, we don't have the pressure difference for the 1st snapshot in all 346 TCs, for the reason that we don't have any previous snapshot to compare to, so we end up having 4152 snapshots with a measurement of the difference of pressure with the previous snapshot. Even the model runs with the most rapid collapse and rapid deepening events combined, 'hot far,' those events only comprise 2.5% of snapshots that have such data.

Model run	Rapid Collapse	Rapid Deepening
Historical	32	10
Cold Near	43	17
Hot Near	47	32
Cold Far	51	26
Hot Far	63	40

Table 3.5: The counting of snapshots that met the criteria of rapid collapse and rapid deepening.

A hypothesis as to why we have more rapid collapse events than rapid deepening events is that many of the rapid collapse events probably are associated with a TC making landfall in CONUS. Since land interaction is one of the fastest ways for a TC to weaken, it stands to reason that many of these events are after a TC makes landfall. Of course, there are cases where hostile environments can weaken a TC quickly with a combination of wind shear, dry air entrainment, or ocean upwelling. But given how our domain is set up around CONUS, landfall is probably the more common factor. Regardless of the mechanism, the fact that both rapid deepening and rapid collapse events increase in the warming scenarios may have implications for hurricane forecasting in the future.

Chapter 4
Discussion and Conclusion

4.1 Summary of findings

Our findings agree with many previous findings of TC-climate research. Further confirmation that a warmer climate will result in more precipitation, particularly in the inner core of TCs, in which we see more precipitation compared to the historical. Both the scenario with the least warming, the 'cold near' scenario, and the one with the most warming, the 'hot far' scenario, see increases in precipitation compared to the historical scenario. The most intense TCs have larger increases in precipitation compared to all TCs. Moderate-intensity TCs also have more increases in precipitation compared to all TCs. Also, the TMQ and precipitation have more instances of increases, whereas dynamical variables like wind are more varied.

The different intensities having different degrees of changes in maximum precipitation might not be surprising, but it might be surprising that the moderate-intensity TCs are the TCs with the greatest increase in maximum precipitation by percent. A hypothesis for this difference might be that the weakest storms are not going to be using all available moisture in the atmosphere local to the storm, while the strongest storms are approaching the point where all the moisture is being used. Meanwhile, the medium-weak and medium-strong storms have large quantities of available moisture and are strong enough to convert atmospheric moisture into precipitation. It is possible that dynamical causes could account for these differences. There has been previous research that has suggested that intensity does seem to play a role in the increases in precipitation and that categorizing by intensity can help resolve the increases in precipitation that are more in line with Clausius-Clapeyron (M. Liu et al., 2019). However, those studies used maximum wind speed to categorize TCs, rather than the MSLP as our analysis did.

We found that most variables had some variety of snapshots that increased or decreased

in value between the historical and warm scenarios. Maximum TMQ is the exception, as almost every single snapshot appeared to have a higher maximum TMQ in all warmer scenarios than the historical. R8 radius had the least percent of snapshots increasing in value, which means that many snapshots are finding smaller TCs in a warmer scenario than the historical one. Most other variables appeared to have a mix of increases and decreases in snapshots for the warmer scenario. Seeing that rapid deepening and rapid collapse events were getting more frequent in warmer scenarios is a finding we note as interesting. However, it is not exactly the same rapid intensification commonly used in operational forecasting, which is usually defined as an increase of at least 35 mph (15-16 m/s) in 24 hours or less.

4.2 Comparison with previous results

Comparing with some of the results from the TC community in Knutson et al., 2020, the benchmark to compare based on previous research for precipitation is 14 % with a range of 6 % to 22 % increase in precipitation as measured by the central part of TC from a +2K global warming from the historical. Given that SSP585 represents a +2-4 K global warming in the 'near' cases and +4-6 K global warming in the 'far' cases, the results for maximum precipitation do appear to match previous research shown in Knutson et al., 2020, particularly if one considers the fact that SSTs in tropical areas represents an area that warms the least comparatively to the globe. A cursory look compared to Clausius-Clapeyron shows that maximum precipitation is either at Clausius-Clapeyron or super Clausius-Clapeyron relationship where the changes are higher than a 7% per 1 K warming. This is not surprising given that it has been noted that extreme precipitation might be at a super Clausius-Clapeyron relationship, even if the mean precipitation increases less than the Clausius-Clapeyron rate (Stansfield & Reed, 2023) (Neelin et al., 2022). One issue is comparing maximum precipitation to the central part of the TC is not a direct comparison.

Given that Patricola and Wehner, 2018 looked at very strong intensity TCs, it would be good to compare our very strong intensity storms of <965 hPa to see better comparisons. For precipitation, we see that Patricola and Wehner, 2018 show the equivalent of the center part of the TC and has Irma and Maria being 27.8% and 36.9% increase in precipitation respectively by the end of the 21st century for the RCP8.5 warming scenario. For our results, 'cold far' and 'hot far' represent the end of the 21st century scenarios and we get a range of 28.5% to 44.4% increase in maximum

precipitation from Table 3.3, which is a range close to the results from Patricola and Wehner, 2018. Of course, this is not an exact comparison given the different metrics used when looking at precipitation. Gutmann et al., 2018 did report changes in the average maximum precipitation and found a 24% increase at the end of the 21st century using RCP8.5. This increase is smaller than the increase we found if we had used the increase in the mean of maximum precipitation for all storms, which was 31.4% in the 'cold far' and 47.2% in the 'hot far' scenarios. Knowing that the kind of storms that Gutmann et al., 2018 analyzed were more likely to be in the medium to very high-intensity TCs, it suggests that my results would be much higher than Gutmann et al., 2018, which would be somewhat surprising given similar methodology from the model and to PGW technique. We would think Gutmann et al., 2018 would have higher precipitation change than our results because they used a smaller spatial resolution, which would help better represent the precipitation in TCs. At the same time, their sample size was small.

As discussed before, a 1-10% increase in maximum wind speed was shown from Knutson et al., 2020. Our results for both 850 hPa winds and surface do seem to match well within those bounds. The 'cold near' scenario is closest to a +2K warming scenario and that ends up having a 2.6% increase in maximum surface wind speeds and a 2.8% increase in maximum 850 hPa winds, which is on the lower end of the range from previous research. For all TCs, the drop in MSLP is slight, but that small drop suggests somewhat more intense TCs. Even at 12 km resolution, there is likely to be some underestimation of both the maximum wind speed and MSLP due to resolution. Looking at the distribution, we can see that the MSLP distribution's lowest values are in the 920 hPa range. However, we have multiple TCs that have likely had lower MSLP just from the IBTrACS data. Furthermore, surface wind speeds end up being up to 50 m/s which would be the borderline inclusion to category 3 on the Saffir-Simpson scale for wind speed, when peak winds being category 5 can be found in multiple TCs in the domain we have.

For the size, the findings from our analysis indicated that, in line with previous research, any size change is small. However, we note that in our case we found a small contraction. Despite using different metrics, the findings were similar to studies that used 12 m/s or even 33 m/s (i.e., hurricane-force winds) (Knutson et al., 2015) (Gutmann et al., 2018). This probably suggests that the size of TCs changing will be small, which has implications for size-dependent TC characteristics like storm surge or damage from the TC's wind field.

4.3 Limitations of this work

One limitation of this study is that we have an assumption that the frequency of TCs is held constant. This study implicitly held frequency constant because we applied the PGW approach. TC research suggests that there might be a slight decrease in the frequency of TCs overall, but the uncertainty is quite high and depends on the basin. So this thesis can inform regarding many changes to TCs, but not to their frequency. Furthermore, there is not a good understanding of what sets the frequency of TCs (Camargo & Wing, 2016). More work needs to be done to TC frequency, but this would likely be done without using a PGW approach (Roberts, Camp, Seddon, Vidale, Hodges, Vannière, et al., 2020).

Unfortunately, we did not have SSP245 scenarios to give a good comparison between SSP245 and SSP585 scenarios from Jones et al., 2023. That would have enabled us to analyze multiple SSP scenarios like how Patricola and Wehner, 2018 was able to look at the four RCP scenarios and a pre-industrial scenario, which is applying PGW by lowering temperature rather than raising the temperature. Unfortunately, we were unable to take advantage of the dynamic change of the warm signal that was allowed in Jones et al., 2023. It could have resulted in better comparisons between individual storms and how they would have changed in a warmer world. Taking advantage of the time dynamic change in the warm signal could give us a better relationship as to what changes are impacted by warming. There are also other factors like wind shear and dry air that might be able to be analyzed using the data from Jones et al., 2023, which could give us more insight into the future changes of TCs due to warming. This gives us a path forward to continue to analyze the Jones et al., 2023 data in the future.

Another limitation is that, while 12 km is high resolution, it might be imperfect to generate TC statistics. Although our precipitation and precipitable water agree with previous research, some of the other PGW studies had small enough spatial resolution such that they were able to run convective permitting models. TCs are formed from convective clouds, so such instances would help improve the representation of precipitation. It is noted that a lack of computing power was the reason for not using convective-permitting resolutions and instead using 12km with a convective parameterization (Jones et al., 2023). We note that this tradeoff permitted 40 years of PGW, which is a very long period to run a PGW scenario compared to past literature. There are instances like Gutmann et al., 2018 and C. Liu et al., 2017 that have run 4.5 km resolution WRF with convective permitting schemes and have run them for 13 years. With more computing

power, a smaller spatial resolution can be run using WRF to try to see if there are further refinements in the changes in TC in warmer scenarios. Yet, broad changes are similar between results that had convective parameterization and results that had convective permitting schemes. We can see this by looking at Gutmann et al., 2018, where similar results were found. Maximum winds are another variable that is underestimated because of high spatial resolution models. Especially in intense TCs, where simulating the eyewall might prove tough without going down to a few kilometers resolution. In summation, in the future, higher-resolution evaluations may be warranted to better tease out changes in the storm's dynamical structure.

With the model itself, since we applied SSTs as a boundary condition, it does not model ocean-atmosphere interactions and ocean effects such as a cold wake that comes from the upwelling of cooler ocean water from the deeper ocean would seem to dampen the strengthening trends by 10-15% (Knutson et al., 2020) (Huang et al., 2015).

Finally, though our sample size was large, storms primarily occurred in the weak and moderate intensity bins, with only 426 snapshots in the intense and very intense intensity bins. Generating a larger sample size for these intense TCs is going to be something that has to be tackled, likely with more simulations and the usage of smaller grid sizes to get enough TC snapshots. At the same time, how much TC representation is enough for analysis to be deemed good enough is probably a question that will be hard to answer.

4.4 Conclusions and future research directions

Overall, our study included a larger sample of TCs than previously published and focused on the broader picture of TCs, not just some specific TCs compared to other PGW studies of TCs. We argue that looking at all of the TCs is important because most TCs are not the intense TCs that are threatening land, but rather weak or moderate intensity TCs. The moisture aspects of the TCs changes are clear, particularly TMQ. Maximum precipitation does tend to increase as well. Dynamical variables such as wind and pressure are a lot less clear in terms of changes in the future. It further suggests that the biggest change for TCs in a warmer climate is that precipitation and moisture-related variables are most likely to be higher. This is more evidence of the general TC consensus of more precipitation from TCs seen in Knutson et al., 2020 and others. We would agree with a medium to high confidence in higher precipitation in TCs, especially for maximum precipitation. Furthermore, intensity seems to be increasing in a warmer world, although individual TCs will depend on different factors and not every TC will be stronger if

repeated in a warmer world. Therefore, we would agree with medium confidence in stronger TCs. Lastly, in our runs TC size does not change materially, so we support lower confidence on whether TC size increases or decreases and therefore higher confidence in no change in TC size.

Some future work that can be performed includes studying other basins for a similar period and seeing how PGW can impact TCs in other basins. Whether or not there are specific patterns that are dependent on the basin could help yield more insight into how or why each basin is different from the other. Also to better understand all TCs, more work should try to look at weaker TCs, especially ones that are of a tropical storm or weak TC strength. Another future work can utilize the data from Jones et al., 2023 to more precisely put warming and TC characteristics into context. Given that we are given a time-involving scenario, it would be good to see whether some variables are more strongly correlated to warming. Our work does suggest that some variables do appear to correlate more with warming such as moisture variables than a variable like R8 (size) or radius of maximum winds. More work can be done with the PGW approach and other model work to better understand the nature of TCs and how they change concerning the warming of the Earth's climate system.

Appendix A
Extra statistics

Below are some additional statistics that were generated during this thesis research.

Mean Statistics of TC Properties					
Variable	Historical	Cold Near	Hot Near	Cold Far	Hot Far
TMQ (mm)	47.4	51.6	52.9	56.6	60.8
Precipitation (mm/hr)	0.51	0.54	0.55	0.58	0.59
Surface winds (m/s)	6.84	6.87	6.89	6.91	6.95
850 hPa winds (m/s)	10.62	10.67	10.68	10.74	10.76

Table A.1: Table of the values of TC properties in the historical case and the four warm scenarios for all TCs.

Many of these variables are mean values for the variables. They are averaged over the composite area of the 10° latitude x 10° longitude. So this area often includes the part outside of the TC. Regardless, many of the signals that are found evaluating the maximum or minimum values of the variables appear to hold when looking at averages of the composites. Although these changes are smaller due to averaging a larger area.

Appendix B
Analysis of other variables with respect to intensity

Below are some other variables that were analyzed using the intensity bins and whether that impacts how much a variable changes in the warmer model runs.

Statistics of Max surface wind via intensity (m/s)					
Variable	Historical	Cold Near	Hot Near	Cold Far	Hot Far
> 1000 hPa	14.2	14.4	14.6	14.9	15.2
		1.4 %	2.8 %	4.9 %	7.0 %
980-1000 hPa	23.3	24.1	24.5	24.8	25.4
		3.4%	5.2 %	6.4 %	9.0 %
965-980 hPa	33.4	34.5	35.3	35.6	36.6
		3.3 %	5.8 %	6.8%	9.8 %
<965 hPa	39.8	40.9	41.4	41.8	43.0
		2.8 %	3.9 %	5.1 %	7.9 %
Statistics of Max 850 hPa winds via intensity (m/s)					
Variable	Historical	Cold Near	Hot Near	Cold Far	Hot Far
> 1000 hPa	21.1	21.6	21.7	22.2	22.5
		2.1 %	2.8 %	4.9 %	6.5 %
980-1000 hPa	36.3	37.7	38.4	38.8	39.6
		3.8 %	5.8 %	6.8 %	9.3 %
965-980 hPa	52.0	53.8	55.2	55.5	57.1
		3.4 %	6.0 %	6.7 %	9.8 %
<965 hPa	63.2	65.2	66.0	66.9	68.9
		3.2 %	4.5 %	5.9 %	9.1 %

Table B.1: Table of the values of average max surface winds and average max 850 hPa winds in the historical case and the four warm scenarios for all TCs. Below each of the warm scenario values is the percent change from the historical that average max surface and 850 hPa winds increased.

Based on the Knutson et al., 2020 review of intensity, which was a 1-10% increase in maximum wind speed with +2K global warming from a pre-industrial baseline, all these values appear to fall within that range, although only cold near comes close to the +2K global warming. Warming does appear to help strengthen max wind speed, although the largest increases in wind speed appear to be in the medium-intensity and the high-intensity bins. If this is the case, then one potential explanation for an increase in the frequency in category 4 and/or 5 TCs with warming can be that TCs that were just below the category 4 threshold and with more warming, were able to strengthen to a higher intensity that crosses the threshold. It makes more sense than a TC that was once a weak storm suddenly becomes a very intense TC, but this is only with warming.

Also, the interesting fact that these medium and high-intensity TCs might be strengthening more than the most intense TCs might make sense from the point of view of Potential Intensity. Since the most intense TCs are closer to the maximum potential intensity based on SST and atmospheric conditions, it probably stands to reason that less intense TCs that are much less away from the maximum potential intensity might have more leeway to strengthen. Of course, despite the percent increase being higher for medium and high-intensity TCs, the largest increase in magnitude is still the very intense TCs. These percentage differences aren't as divergent as the maximum precipitation, but some differences are interesting to note. It shows the potential need to separate TCs by intensity due to different dynamics at play.

B.1 Composite plots with intensity, weak vs. strong for precipitation

Looking at how taking composites of intensity bins could give us some insight as to what might be different between different TC intensities. Figure B.1 is the composite of the weak intensity TCs of >1000 hPa and the changes in the precipitation in the warm scenarios. As expected, the weak TCs do not have strong winds with the 8 m/s being irregularly shaped and the 12 m/s winds are a small part of the TC to the east of the center of the TC. The maximum precipitation is northeast of the center of the TC, which is pretty similar to the composite of all TCs. Given that the weak TCs comprised 2966 snapshots, which is 66% of all snapshots, it is expected that there will be similarities to the composite of all TCs. The changes to precipitation in the warm scenarios seem to be small and concentrated near the center of the weak TC, surrounded by the 8 m/s

contour curve. A similar pattern emerges where the warmest scenario, hot far, has the most robust increase in precipitation.

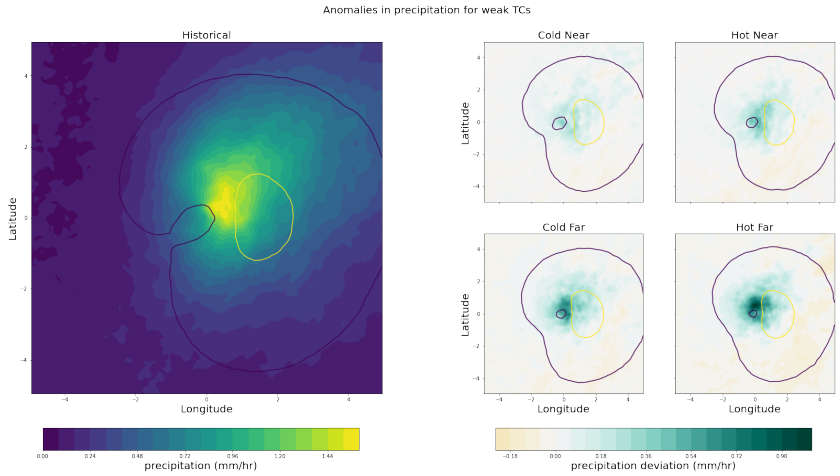

Figure B.1: On the left is the historical average precipitation for weak TCs. On the right is a four-panel plot of 4 warming scenarios that show how the composite precipitation changes for weak TCs.

Figure B.2 is the composite of the very intense TCs of <965 hPa and the changes in the precipitation in the 4 warm scenarios. One thing to note is that the 8 m/s contour curve is nowhere to be seen, which means almost the entire composite grid for very intense TCs is 8 m/s or higher in the 850 hPa winds. The 12 m/s winds encompass a lot of the composite domain as well. For these very intense TCs, we can see the ring of precipitation, which is the eyewall, and the relative dry spot in the center of the TC, which is the eye. The maximum precipitation is on the northeast quadrant of the TC in the eyewall. As for the changes in precipitation, the changes are concentrated in the eyewall and the surrounding areas. The precipitation change does seem to suggest a decrease in the eyewall radius, which does match the findings of having a smaller radius of maximum winds. There are also some interesting changes outside of the eyewall, which might be the intensification or the establishment of rain bands outside of the TC center. Even the least warm scenario, cold near, has some banding that sticks out in the change.

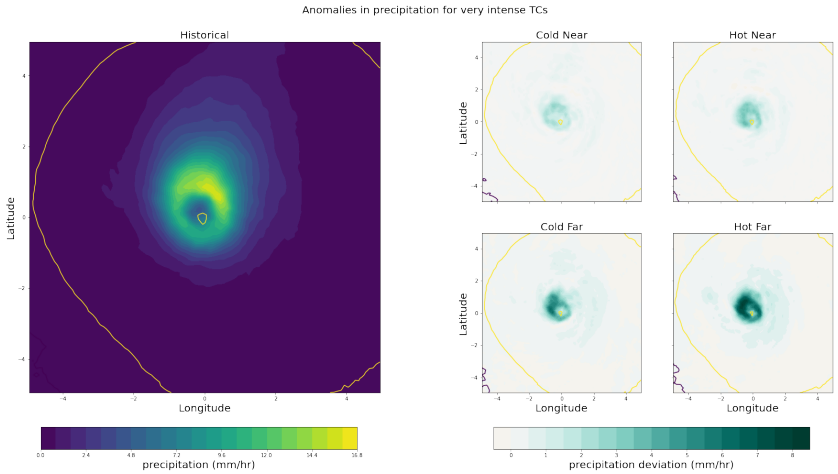

Figure B.2: On the left is the historical average precipitation for very intense TCs. On the right is a four-panel plot of 4 warming scenarios that show how the composite precipitation changes for very intense TCs.

Bibliography

Camargo, S. J., & Wing, A. A. (2016). Tropical cyclones in climate models. *Wiley Interdisciplinary Reviews: Climate Change*, *7*(2), 211–237.

Davis, C. (2018). Resolving tropical cyclone intensity in models. *Geophysical Research Letters*, *45*(4), 2082–2087.

Davis, C. A., & Bosart, L. F. (2003). Baroclinically induced tropical cyclogenesis. *Monthly Weather Review*, *131*(11), 2730–2747.

DeHart, J. C., Houze, R. A., & Rogers, R. F. (2014). Quadrant distribution of tropical cyclone inner-core kinematics in relation to environmental shear. *Journal of the Atmospheric Sciences*, *71*(7), 2713–2732.

Delfino, R. J., Vidale, P. L., Bagtasa, G., & Hodges, K. (2023). Response of damaging philippines tropical cyclones to a warming climate using the pseudo global warming approach. *Climate Dynamics*, 1–25.

DeMaria, M., & Kaplan, J. (1994). Sea surface temperature and the maximum intensity of atlantic tropical cyclones. *Journal of climate*, *7*(9), 1324–1334.

Emanuel, K., DesAutels, C., Holloway, C., & Korty, R. (2004). Environmental control of tropical cyclone intensity. *Journal of the atmospheric sciences*, *61*(7), 843–858.

Emanuel, K. A. (1986). An air-sea interaction theory for tropical cyclones. part i: Steady-state maintenance. *Journal of Atmospheric Sciences*, *43*(6), 585–605.

Eyring, V., Bony, S., Meehl, G. A., Senior, C. A., Stevens, B., Stouffer, R. J., & Taylor, K. E. (2016). Overview of the coupled model intercomparison project phase 6 (cmip6) experimental design and organization. *Geoscientific Model Development*, *9*(5), 1937–1958.

Fu, Q., Manabe, S., & Johanson, C. M. (2011). On the warming in the tropical upper troposphere: Models versus observations. *Geophysical Research Letters*, *38*(15).

Gray, W. M. (1968). Global view of the origin of tropical disturbances and storms. *Monthly Weather Review*, *96*(10), 669–700.

Gutmann, E. D., Rasmussen, R. M., Liu, C., Ikeda, K., Bruyere, C. L., Done, J. M., Garrè, L., Friis-Hansen, P., & Veldore, V. (2018). Changes in hurricanes from a 13-yr convection-permitting pseudo–global warming simulation. *Journal of Climate*, *31*(9), 3643–3657.

Held, I. M., & Soden, B. J. (2006). Robust responses of the hydrological cycle to global warming. *Journal of climate*, *19*(21), 5686–5699.

Hersbach, H., Bell, B., Berrisford, P., Hirahara, S., Horányi, A., Muñoz-Sabater, J., Nicolas, J., Peubey, C., Radu, R., Schepers, D., et al. (2020). The era5 global

reanalysis. *Quarterly Journal of the Royal Meteorological Society*, *146*(730), 1999–2049.

Hill, K. A., & Lackmann, G. M. (2009). Influence of environmental humidity on tropical cyclone size. *Monthly Weather Review*, *137*(10), 3294–3315.

Hill, K. A., & Lackmann, G. M. (2011). The impact of future climate change on TC intensity and structure: A downscaling approach. *Journal of Climate*, *24*(17), 4644–4661.

Huang, P., Lin, I.-I., Chou, C., & Huang, R.-H. (2015). Change in ocean subsurface environment to suppress tropical cyclone intensification under global warming. *Nature Communications*, *6*(1), 7188.

Jones, A. D., Rastogi, D., Vahmani, P., Stansfield, A. M., Reed, K. A., Thurber, T., Ullrich, P. A., & Rice, J. S. (2023). Continental United States climate projections based on thermodynamic modification of historical weather. *Scientific Data*, *10*(1), 664.

Kanada, S., Wada, A., & Sugi, M. (2013). Future changes in structures of extremely intense tropical cyclones using a 2-km mesh nonhydrostatic model. *Journal of climate*, *26*(24), 9986–10005.

Knapp, K. R., Diamond, H. J., Kossin, J. P., Kruk, M. C., & Schreck, C. J. I. (2018). *International Best Track Archive for Climate Stewardship (IBTrACS) Project, Version 4*. https://www.ncei.noaa.gov/access/metadata/landing-page/bin/iso?id=gov.noaa.ncdc:C01552

Knapp, K. R., Kruk, M. C., Levinson, D. H., Diamond, H. J., & Neumann, C. J. (2010). The international best track archive for climate stewardship (IBTrACS) unifying tropical cyclone data. *Bulletin of the American Meteorological Society*, *91*(3), 363–376.

Knutson, T. R., Camargo, S. J., Chan, J. C., Emanuel, K., Ho, C.-H., Kossin, J., Mohapatra, M., Satoh, M., Sugi, M., Walsh, K., et al. (2020). Tropical cyclones and climate change assessment: Part ii: Projected response to anthropogenic warming. *Bulletin of the American Meteorological Society*, *101*(3), E303–E322.

Knutson, T. R., Sirutis, J. J., Zhao, M., Tuleya, R. E., Bender, M., Vecchi, G. A., Villarini, G., & Chavas, D. (2015). Global projections of intense tropical cyclone activity for the late twenty-first century from dynamical downscaling of cmip5/rcp4.5 scenarios. *Journal of Climate*, *28*(18), 7203–7224.

Lackmann, G. M. (2015). Hurricane Sandy before 1900 and after 2100. *Bulletin of the American Meteorological Society*, *96*(4), 547–560.

Landsea, C. W., Vecchi, G. A., Bengtsson, L., & Knutson, T. R. (2010). Impact of duration thresholds on atlantic tropical cyclone counts. *Journal of Climate*, *23*(10), 2508–2519.

Liu, C., Ikeda, K., Rasmussen, R., Barlage, M., Newman, A. J., Prein, A. F., Chen, F., Chen, L., Clark, M., Dai, A., et al. (2017). Continental-scale convection-permitting modeling of the current and future climate of north america. *Climate Dynamics*, *49*, 71–95.

Liu, M., Vecchi, G. A., Smith, J. A., & Knutson, T. R. (2019). Causes of large projected increases in hurricane precipitation rates with global warming. *NPJ climate and atmospheric science*, *2*(1), 38.

Mendelsohn, R., Emanuel, K., Chonabayashi, S., & Bakkensen, L. (2012). The impact of climate change on global tropical cyclone damage. *Nature climate change*, *2*(3), 205–209.

Nakamura, R., Shibayama, T., Esteban, M., & Iwamoto, T. (2016). Future typhoon and storm surges under different global warming scenarios: case study of typhoon Haiyan (2013). *Natural Hazards*, *82*, 1645–1681.

Needham, H. F., & Keim, B. D. (2014). An empirical analysis on the relationship between tropical cyclone size and storm surge heights along the us gulf coast. *Earth Interactions*, *18*(8), 1–15.

Neelin, J. D., Martinez-Villalobos, C., Stechmann, S. N., Ahmed, F., Chen, G., Norris, J. M., Kuo, Y.-H., & Lenderink, G. (2022). Precipitation extremes and water vapor: Relationships in current climate and implications for climate change. *Current Climate Change Reports*, *8*(1), 17–33.

O'Gorman, P. A. (2015). Precipitation extremes under climate change. *Current climate change reports*, *1*, 49–59.

Patricola, C. M., & Wehner, M. F. (2018). Anthropogenic influences on major tropical cyclone events. *Nature*, *563*(7731), 339–346.

Rasmussen, R., Liu, C., Ikeda, K., Gochis, D., Yates, D., Chen, F., Tewari, M., Barlage, M., Dudhia, J., Yu, W., et al. (2011). High-resolution coupled climate runoff simulations of seasonal snowfall over colorado: A process study of current and warmer climate. *Journal of Climate*, *24*(12), 3015–3048.

Riahi, K., Van Vuuren, D. P., Kriegler, E., Edmonds, J., O'neill, B. C., Fujimori, S., Bauer, N., Calvin, K., Dellink, R., Fricko, O., et al. (2017). The shared socioeconomic pathways and their energy, land use, and greenhouse gas emissions implications: An overview. *Global environmental change*, *42*, 153–168.

Roberts, M. J., Camp, J., Seddon, J., Vidale, P. L., Hodges, K., Vanniere, B., Mecking, J., Haarsma, R., Bellucci, A., Scoccimarro, E., et al. (2020). Impact of model resolution on tropical cyclone simulation using the highresmip–primavera multimodel ensemble. *Journal of Climate*, *33*(7), 2557–2583.

Roberts, M. J., Camp, J., Seddon, J., Vidale, P. L., Hodges, K., Vannière, B., Mecking, J., Haarsma, R., Bellucci, A., & Scoccimarro, E. (2020). Projected future changes in tropical cyclones using the cmip6 highresmip multimodel ensemble. *Geophysical research letters*, *47*(14), e2020GL088662.

Schär, C., Frei, C., Lüthi, D., & Davies, H. C. (1996). Surrogate climate-change scenarios for regional climate models. *Geophysical Research Letters*, *23*(6), 669–672.

Schenkel, B. A., Lin, N., Chavas, D., Oppenheimer, M., & Brammer, A. (2017). Evaluating outer tropical cyclone size in reanalysis datasets using quikscat data. *Journal of Climate*, *30*(21), 8745–8762.

Scoccimarro, E., Gualdi, S., Villarini, G., Vecchi, G. A., Zhao, M., Walsh, K., & Navarra, A. (2014). Intense precipitation events associated with landfalling tropical cyclones

in response to a warmer climate and increased CO2. *Journal of climate*, *27*(12), 4642–4654.

Service, N. P. (2019). https://www.nps.gov/articles/saffir-simpson-hurricane-scale.htm

Skamarock, W. C., Klemp, J. B., Dudhia, J., Gill, D. O., Liu, Z., Berner, J., Wang, W., Powers, J., Duda, M., Barker, D., & Huang, X. (2021). A description of the advanced research wrf version 4.3. *NCAR tech. note ncar/tn-556+ str*.

Smith, A. B., & Katz, R. W. (2013). Us billion-dollar weather and climate disasters: Data sources, trends, accuracy and biases. *Natural hazards*, *67*(2), 387–410.

Stansfield, A. M., & Reed, K. A. (2023). Global tropical cyclone precipitation scaling with sea surface temperature. *npj Climate and Atmospheric Science*, *6*(1), 60.

Tomassini, L., Willett, M., Sellar, A., Lock, A., Walters, D., Whitall, M., Sanchez, C., Heming, J., Earnshaw, P., Rodriguez, J. M., et al. (2023). Confronting the convective gray zone in the global configuration of the met office unified model. *Journal of Advances in Modeling Earth Systems*, *15*(5), e2022MS003418.

Tuleya, R. E., Bender, M., Knutson, T. R., Sirutis, J. J., Thomas, B., & Ginis, I. (2016). Impact of upper-tropospheric temperature anomalies and vertical wind shear on tropical cyclone evolution using an idealized version of the operational gfdl hurricane model. *Journal of the Atmospheric Sciences*, *73*(10), 3803–3820.

Ullrich, P. A., & Zarzycki, C. M. (2017). TempestExtremes: A framework for scale-insensitive pointwise feature tracking on unstructured grids. *Geoscientific Model Development*, *10*(3), 1069–1090.

Ullrich, P. A., Zarzycki, C. M., McClenny, E. E., Pinheiro, M. C., Stansfield, A. M., & Reed, K. A. (2021). TempestExtremes v2. 1: a community framework for feature detection, tracking, and analysis in large datasets. *Geoscientific Model Development*, *14*(8), 5023–5048.

Vecchi, G. A., & Soden, B. J. (2007). Increased tropical atlantic wind shear in model projections of global warming. *Geophysical Research Letters*, *34*(8).

Wang, C.-C., Lin, B.-X., Chen, C.-T., & Lo, S.-H. (2015). Quantifying the effects of long-term climate change on tropical cyclone rainfall using a cloud-resolving model: Examples of two landfall typhoons in taiwan. *Journal of Climate*, *28*(1), 66–85.

Wehner, M. (2021). Simulated changes in tropical cyclone size, accumulated cyclone energy and power dissipation index in a warmer climate. *Oceans*, *2*(4), 688–699.

Zhai, A. R., & Jiang, J. H. (2014). Dependence of us hurricane economic loss on maximum wind speed and storm size. *Environmental Research Letters*, *9*(6), 064019.